ACS Partner Journal

CHEMICAL & BIOMEDICAL IMAGING

pubs.acs.org/ChemBioImaging

Article

Smart Persistent Luminescence Imaging for Early Diagnosis of Drug-Induced Liver Injury

Feng Zhang, Liang Song,* Ye Lin, Zhengxia Yang, Junpeng Shi, Quan Yuan,* and Yun Zhang*

Cite This: *Chem. Biomed. Imaging* 2025, 3, 77−84

Read Online

ACCESS | Metrics & More | Article Recommendations | Supporting Information

ABSTRACT: Drug-induced liver injury (DILI) has the potential to cause severe hepatitis and increases the risk of death which remains unresolved in current medical practice. During DILI, the H_2O_2 level is upregulated in the liver. Conventional blood tests fail to offer early and real-time visualization of DILI in vivo. Here we report a smart persistent luminescent approach to evaluate DILI in vivo using persistent luminescence nanoprobes which are conjugated with single-stranded DNA containing Ferrocene (Fc). Upon injection, these nanoprobes mainly accumulate in the liver and the persistent luminescence of nanoprobes remains suppressed owing to energy transfer to the ferrocene. The presence of H_2O_2 during DILI initiates the Fenton reaction to induce cleavage of DNA chains, and the ferrocene dissociates from the probes, leading to fast restoration of the persistent luminescence. The DILI imaging results revealed a signal-to-noise ratio of 20.9, approximately 10 h earlier than the serum-based detection methods. With its exceptional sensitivity, high signal-to-noise ratio, and real-time imaging capabilities, this smart persistent luminescent approach holds great promise for the early diagnosis of DILI.

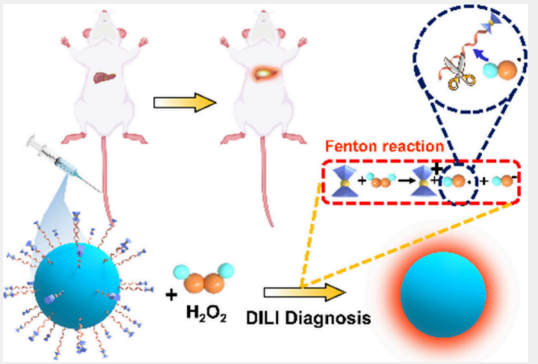

KEYWORDS: *Nanoprobe, Ferrocene, NIR-PLNPs, Early imaging of DILI, Fenton reaction*

INTRODUCTION

Drug-induced liver injury (DILI) is a common adverse reaction caused by medications,[1] which can lead to severe hepatic dysfunction, failure, and even mortality.[2] Therefore, it represents a critical issue that requires attention in clinical practice.[3] Currently, the gold standard for diagnosing DILI in clinical settings is quantifying hepatic enzymes in the bloodstream, such as alanine aminotransferase (ALT) and aspartate aminotransferase (AST).[4] However, these markers fail to provide early prediction of DILI and are often only detectable after liver damage has already occurred.[5,6] Moreover, their lack of specificity is evident as ALT and AST can also indicate skeletal muscle injury.[7,8] Due to the lack of early stage symptoms in DILI, the absence of a highly specific diagnostic marker results in missed or misdiagnosed cases, posing challenges for clinicians to accurately assess the incidence of DILI.[9] Furthermore, DILI can lead to severe hepatitis and carry a risk of fatality. Therefore, an urgent need exists for the development of a highly specific method capable of early detection of DILI.

Research has demonstrated that excessive drug exposure during hepatic cellular metabolism undergoes enzymatic biotransformation through a series of oxidation reactions, resulting in the generation of highly reactive intermediate metabolites. These excessive metabolites deplete glutathione within the cytoplasm and mitochondria, leading to an overproduction of reactive oxygen species (ROS),[10] such as H_2O_2, within the mitochondria. Consequently, this exacerbates oxidative stress reactions, ultimately causing severe hepatotoxicity and liver damage.[11] Therefore, endogenous H_2O_2 can serve as an early in situ biomarker for DILI.[12−14] Currently, various fluorescence probes have been developed and employed for the detection of H_2O_2 in biological systems.[15−18] However, most of these probes are small organic molecules that exhibit susceptibility to photobleaching and possess poor photostability.[10] Moreover, the reported probes for endogenous H_2O_2 imaging rely on external light sources, which give rise to autofluorescence signals from the biological system, thereby reducing imaging sensitivity. Consequently, there still exist limitations in achieving early and accurate diagnosis of DILI.

Near-infrared persistent luminescence nanoparticles (NIR-PLNPs) are a class of nanomaterials capable of emitting continuous near-infrared light, even post excitation light cessation.[19,20] Their utilization in biomedical imaging circumvents autofluorescence signal interference arising from excitation light sources and enhances imaging sensitivity.[21,22]

Received: July 22, 2024
Revised: September 30, 2024
Accepted: October 2, 2024
Published: November 15, 2024

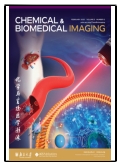

https://doi.org/10.1021/cbmi.4c00056
Chem. Biomed. Imaging 2025, 3, 77−84

In this study, we modified the surface of ZGGO:Cr NIR-PLNPs with single-stranded DNA containing a quenching group, ferrocene, to fabricate a smart persistent luminescent approach for highly sensitive imaging of DILI (Scheme 1).

Scheme 1. Schematic Illustration of H_2O_2-Responsive NIR-PLNPs for Diagnosis of DILI In Vivo

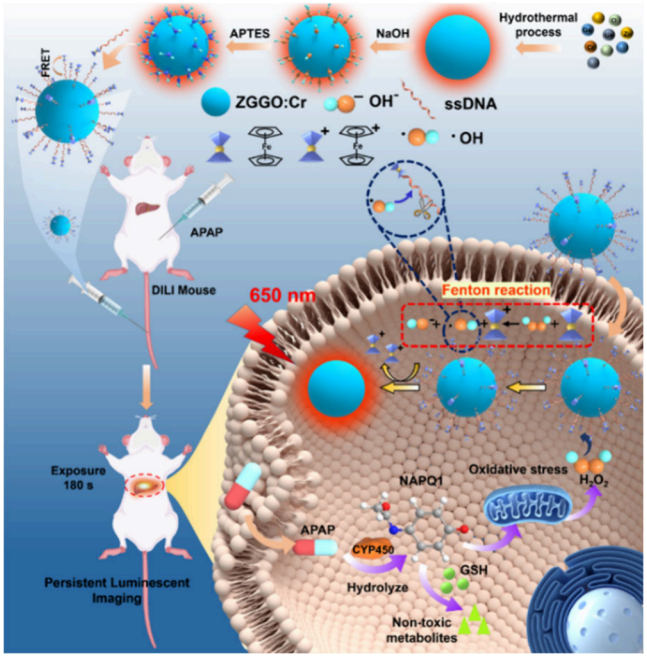

After reacting with H_2O_2, this nanoprobe effectively restores the near-infrared persistent luminescence signal of ZGGO:Cr, thereby facilitating real-time monitoring of DILI in live animal models. We successfully validated its response to H_2O_2 in vitro and demonstrated its application for the detection of endogenous H_2O_2. In acute DILI mouse models induced by acetaminophen (APAP), we achieved early diagnosis imaging of DILI in mice, which was approximately 10 h earlier than serum-based detection methods. Thus, this nanoprobe exhibits promising potential as a valuable tool for early diagnosis of DILI.

EXPERIMENTAL SECTION

Synthesis of ZGGO:Cr

$Zn_{1.2}Ga_{1.6}Ge_{0.2}O_4:Cr_{0.005}$(ZGGO:Cr) was synthesized as follows: First, 1.2 mmoL of $Zn(NO_3)_2$, 1.6 mmoL of $Ga(NO_3)_3$, 0.2 mmoL of Na_2GeO_3, and 0.0075 mmoL of $Cr(NO_3)_3$ were dissolved in 11 mL of deionized water. Then, ammonium hydroxide (28 wt %) was rapidly added to the solution and vigorously stirred to adjust the pH to around 6.5. The mixture was stirred at room temperature for 2 h and then transferred to a reaction vessel. The reaction was carried out at 220 °C for 12 h. After the oven temperature returned to room temperature, the reaction solution was transferred to a centrifuge tube and washed three times with deionized water at 10,000 rpm. The sample was then dried and stored for future use.

Surface Modification of ZGGO:Cr

Twenty mg of the material was added to a 50 mL solution of NaOH (5 mM) and sonicated for 30 min. It was then stirred at room temperature for 24 h and centrifuged three times at 10,000 rpm for 10 min each. The modified ZGGO:Cr−OH was weighed (30 mg) and dispersed in 15 mL of DMF solution through sonication. The dispersion was transferred to a 50 mL round-bottom flask, and 300 μL of APTES was added. The mixture was stirred at 80 °C for 24 h. The sample was then washed three times with ethanol and deionized water at 10,000 rpm. After drying, amino-modified ZGGO:Cr was successfully obtained

Synthesis of ZGGO:Cr-Fc Probe

Single-stranded DNA modified with ferrocene, which had a carboxyl group at one end, was activated. Thirty μg of the DNA was dissolved in MES solution and mixed by shaking. After adding EDC, the mixture was stirred for 10 min and then NHS was added and stirred for 45−60 min. The pH was adjusted to 7−8 with $NaHCO_3$. Then, ZGGO:Cr-NH_2 was added and stirred overnight. The sample was centrifuged at 10,000 rpm for 10 min.

Spectral Measurements

The luminescence intensity of ZGGO:Cr-Fc nanoprobes (1 mg/mL) was measured at different H_2O_2 concentrations. The ZGGO:Cr-Fc (1 mg/mL) nanoprobe was dispersed in 2 mL PBS buffer solution and its pH was adjusted to 5.And then add different concentrations of H_2O_2 (5 μM, 50 μM, 100 μM, 150 μM, 200 μM). After incubating for 2 h, the samples were centrifuged and the supernatant was removed. PBS buffer solution was added again before measuring the fluorescence spectra. The fluorescence spectra of ZGGO:Cr-Fc nanoprobes (1 mg/mL) were also measured after incubating with GSH, Na^+, Fe^{2+}, Fe^{3+}, NO_2^-, NO_3^-, SO_3^{2-}, SO_4^{2-}, HCO_3^-, CH_2COO^-, Mg^{2+}, Ca^{2+}, and K^+ (200 μM) for 2 h. The samples were excited with a 659 nm light-emitting diode (LED) at an intensity of 40 mW/cm^{-2} for 5 min, and the spectra were measured at intervals of 8 s using a spectrometer.

Cell Toxicity Assay

The standard cell counting kit-8(CCK-8) assay was used to measure the viability of normal HepG2 liver cancer cells and MCF-10A cells. HepG2 cells and MCF-10A cells were seeded in a 96-well plate at a density of 5×10^3 cells/well and cultured for 24 h at 37 °C with 5% CO_2. The cells were then treated with different doses of ZGGO:Cr-Fc for 24 h. The culture medium was replaced with fresh medium containing 10% CCK-8. After incubating for 1 h, the cells were analyzed using an enzyme-linked immunosorbent assay reader.

Cell Experiments

Cell imaging was performed to verify the endogenous H_2O_2 concentration in HepG2 cells after different treatments. HepG2 cells were divided into three groups: Group 1, cells cultured normally; Group 2, cells pretreated with 1000 μM APAP for 12 h; Group 3, cells pretreated with NAC (500 μM) for 2 h, followed by treatment with APAP (1000 μM) for 12 h. Finally, 100 μL ZGGO:Cr-Fc probe (1 mg/mL) was added and incubated for 2 h. Fluorescence imaging was performed using an IVIS Lumina II in vivo imaging system (Caliper Life Science, Inc., USA) after illuminating the mice with a 659 nm LED at an intensity of 40 mW/cm^{-2} for 5 min. The exposure time was 100 s.

Animal Models

Female Balb/c mice (6 weeks old) were obtained from GemPharmatech LLC. For the drug-induced liver injury model, acetaminophen (APAP) was injected into the mice at a dose of 300 mg/kg via intraperitoneal injection, followed by a drug injection into the tail vein after 1 h. For the treatment model, NAC (150 mg/kg) was injected 1 h before APAP (300 mg/kg) injection. The control group received an equivalent dose of PBS via intraperitoneal injection.

In Vivo Persistent Luminescence Imaging

200 μL nanoprobes (1 mg/mL) of PBS buffer solution was injected into the tail vein of the mice. Under 2% gas anesthesia, the mice were illuminated with a 659 nm LED at an intensity of 40 mW/cm^{-2} for 5 min, and the persistent luminescence (PersL) images were recorded at different time points (10, 20, 40, 60 min) using an IVIS Lumina II in vivo imaging system. The major organs (heart, liver, spleen, lungs, and kidneys) were dissected and imaged with an exposure time of 180 s. All images were processed using Living Image software (Caliper Life Science, Inc., Version 4.3.1).

https://doi.org/10.1021/cbmi.4c00056
Chem. Biomed. Imaging 2025, 3, 77−84

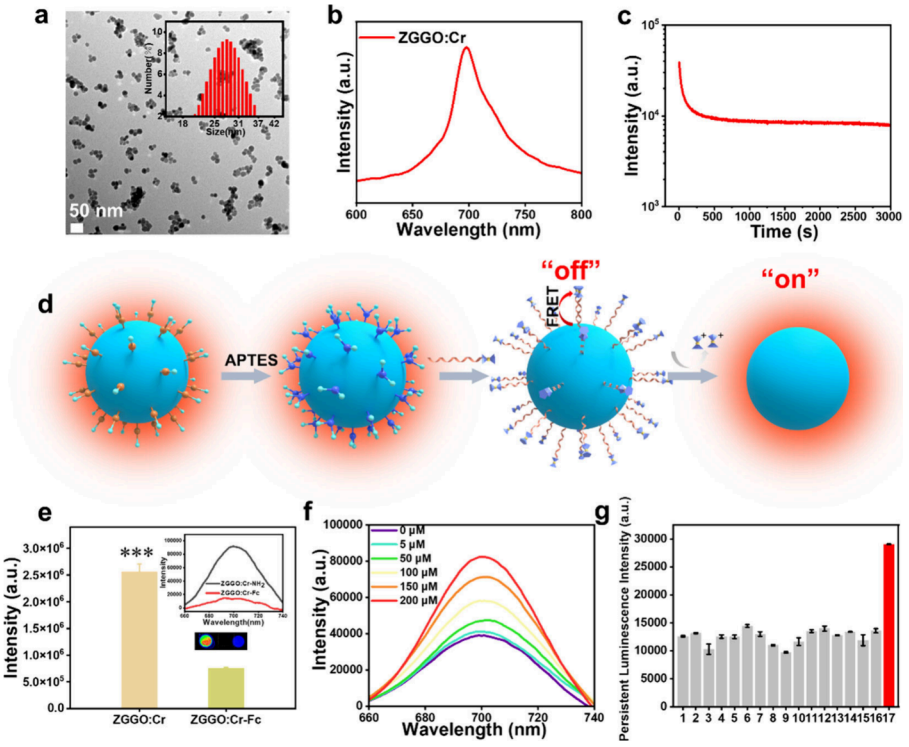

Figure 1. (a) TEM image and particle size distribution of the nanoparticles. (b) Emission peak of ZGGO:Cr. (c) Decay curve of PersL emission at 696 nm after 5 min of LED irradiation at 659 nm. (d) ZGGO:Cr-Fc "off-on" mechanism. (e) Intensity comparison and spectral changes of PersL emission before and after surface modification of ZGGO:Cr with Fc, as observed with a CCD camera. ***$p < 0.001$, $n = 3$. (f) Postreaction PersL emission intensity of ZGGO:Cr-Fc with different concentrations of H_2O_2. (g) Fluorescence intensity of ZGGO:Cr-Fc in the presence of different analytes: 1, blank; 2, GSH; 3, NO_2^-; 4, HCO_3^-; 5, NO_3^-; 6, CH_2COO^-; 7, Na^+; 8, Fe^{3+}; 9, SO_4^{2-}; 10, SO_3^{2-}; 11, Mg^{2+}; 12, Ca^{2+}; 13, Fe^{2+}; 14, K^+; 15, APAP; 16, NAC; 17 H_2O_2,. (200 μmoL/L).

RESULTS AND DISCUSSION

ZGGO:Cr Synthesis, Modification, and Response to H_2O_2

We synthesized $Zn_{1.2}Ga_{1.6}Ge_{0.2}O_4:Cr_{0.005}$ through a hydrothermal synthesis method. The particle size and distribution were observed using TEM. As shown in Figure 1a, the synthesized nanoparticles exhibited excellent dispersion with a uniform diameter of 25 ± 5 nm. Elemental analysis using high-angle annular dark-field scanning and EDS confirmed the presence of Zn, Ga, Ge, O, and Cr as the main constituents of ZGGO:Cr (Figure S1). Additionally, XRD analysis confirmed the high crystallinity and typical cubic spinel structure of ZGGO:Cr, indicating the successful synthesis of the desired persistent luminescence nanoparticles (Figure S2).And the ZGGO:Cr were effectively dispersed and maintained stability in both serum and cell medium environments (Figure S3)..

Excellent PersL performance of PLNPs is very important to achieve early high-sensitivity imaging of DILI. As the excitation and emission spectra shown (Figure S4), the photoluminescence of ZGGO:Cr can be excited by a light source around 659 nm. Upon 659 nm LED light irradiation, ZGGO:Cr exhibited a strong NIR PersL emission peak at 696 nm (Figure 1b). Furthermore, ZGGO:Cr exhibited a slow NIR PersL decay and could be repeatedly excited by 659 nm LED (Figure 1c and Figure S5). To further investigate the NIR PersL properties of ZGGO:Cr, we employed a charge-coupled device (CCD) camera to measure its NIR PersL. Following irradiation with a 659 nm LED for 5 min, the changes in PersL intensity over the decay time were illustrated in (Figure S5a). Remarkably, even after 30 min, the NIR PersL emitted from ZGS was still detectable using the CCD camera.

In order to achieve susceptible and specific detection of endogenous H_2O_2, the development of H_2O_2-responsive "off-on" nanoprobes holds significant importance. Therefore, we employed a single-stranded DNA linkage to connect ferrocene with nanoparticles, creating an H_2O_2-responsive "off-on" persistent luminescence nanoprobe based on the Fenton reaction (Figure 1d). The ZGGO: Cr was initially functionalized with hydroxyl groups, followed by amino-functionalization using APTES. Subsequently, an amide reaction was employed to couple carboxyl-modified single-stranded DNA, with ferrocene attached at one end, to the amino groups of ZGGO:Cr. The change in zeta potential from negative to positive from the hydroxyl-modified to amino-modified state, and then from positive to negative after coupling with ferrocene, indicated the successful attachment of ferrocene-modified single-stranded DNA to ZGGO:Cr (Figure S6). We performed TEM and DLS of the nanomaterial ZGGO:Cr-Fc, the particle size of the nanoprobe becomes larger after modifying and the particle size is about 130 nm (Figure S7). Additionally, we observed a significant decrease in the persistent luminescence intensity of ZGGO:Cr upon attachment of ferrocene-modified single-stranded DNA, indicating quenching induced by ferrocene (Figure 1e). This quenching effect arises from the spectral overlap between the absorption peak of ferrocene and the emission peak of ZGGO:Cr (Figure S8). The results indicate the successful engineering of a nanoprobe in an "off" state, designated as ZGGO:Cr-Fc. Then we validated the response of ZGGO:Cr-Fc to H_2O_2 in vitro, specifically its ability to transition from the "off" state to the "on" state. Prior to this, H_2O_2 was introduced into an

https://doi.org/10.1021/cbmi.4c00056
Chem. Biomed. Imaging 2025, 3, 77−84

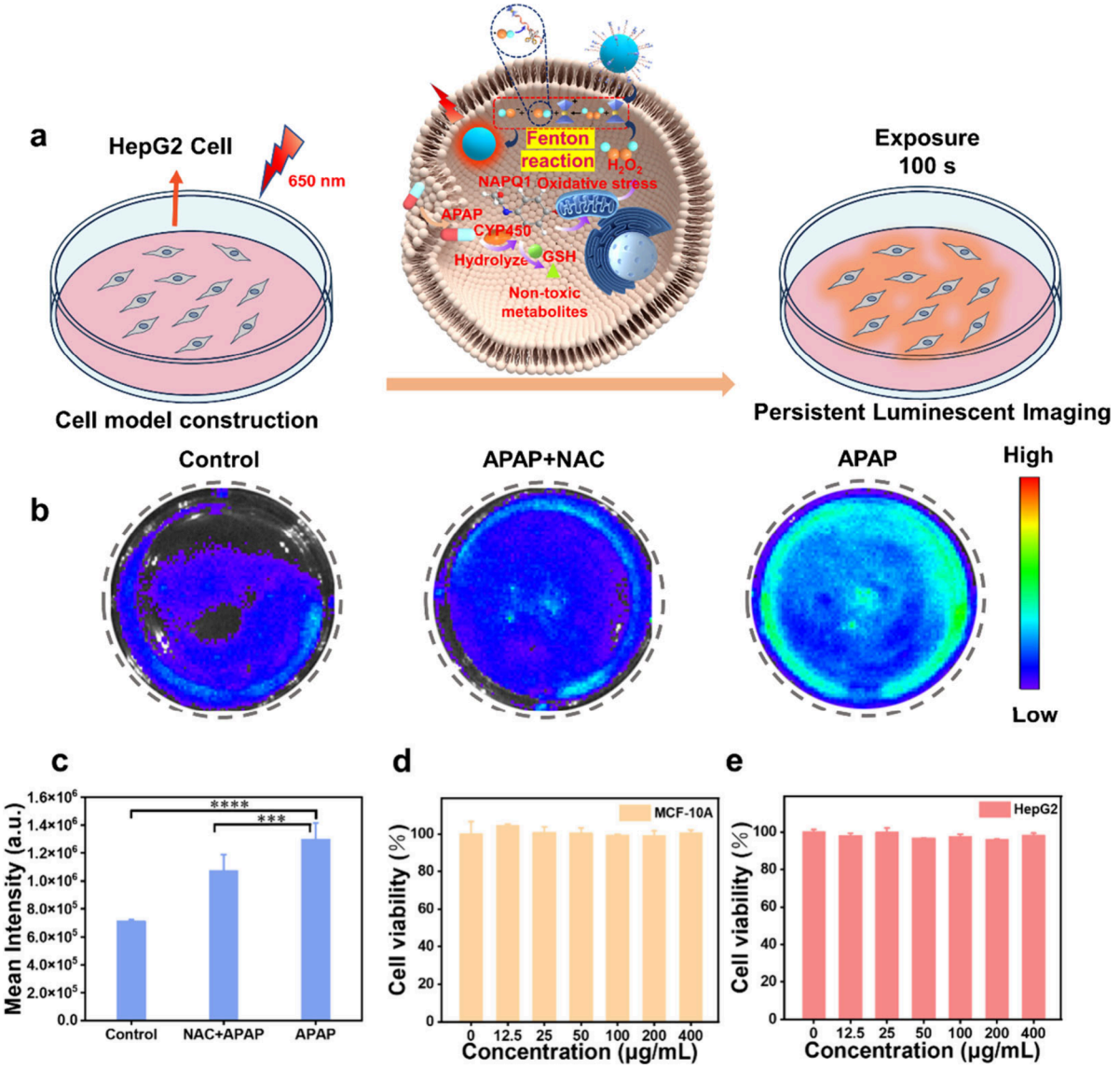

Figure 2. (a) Pretreatment and imaging process of HepG2 cells. (b) Imaging results of HepG2 cells in different groups. (c) Statistical fluorescence intensity of HepG2 cells in different groups. ****$p < 0.0001$, $n = 3$, ***$p < 0.001$, $n = 3$. (d, e) Cytotoxicity of MCF-10A cells and HepG2 cells.

unmodified ZGGO:Cr PBS buffer solution, and it was observed that the persistent luminescence intensity of ZGGO:Cr remained unaffected. This observation indicates that the material itself does not exhibit a response toward H_2O_2 (Figure S9). Subsequently, we introduced different concentrations of H_2O_2 into a PBS buffer solution containing the prepared ZGGO:Cr-Fc nanoprobe. In the solution system, upon encountering H_2O_2, ferrocene initiates the Fenton reaction,[23] leading to the generation of hydroxyl radicals. These highly reactive species effectively cleave single-stranded DNA molecules. Consequently, ferrocene dissociates from the nanoprobe, facilitating the recovery of persistent luminescence signal in ZGGO:Cr. As shown in Figure 1f, following incubation of ZGGO:Cr-Fc in a PBS solution with H_2O_2, the centrifuged sample exhibited an enhanced persistent luminescence intensity. Furthermore, the fluorescence intensity increased gradually increased with escalating H_2O_2 concentration and the LOD is 4.469 μmoL/L. To investigate the specificity of ZGGO:Cr-Fc for H_2O_2 detection, we measured the persistent luminescence spectra in the presence of other substances under identical experimental conditions (Figure 1g). Remarkably, only H_2O_2 induced a significant enhancement in persistent luminescence emission, while other substances exhibited negligible interference. indicating the high selectivity of ZGGO:Cr-Fc for H_2O_2. These findings unequivocally demonstrate the exceptional selectivity of ZGGO:Cr-Fc toward H_2O_2.

The luminescent stability of the ZGGO:Cr-Fc nanoprobe was further evaluated under various conditions, including different ion concentrations, pH levels, and in cell culture media containing 10% (v/v) fetal bovine serum. Remarkably, the results demonstrated exceptional luminescent stability of the nanoprobe (Figure S10). These results demonstrate that ZGGO:Cr-Fc exhibits excellent NIR PersL performance, suggesting its great potential for early high-sensitivity diagnosis of DILI.

ZGGO:Cr-Fc Nanoprobe: Safety Assessment and Response to H_2O_2 in Liver Injury Cell Model

DILI commonly arises from intentional or accidental overdose. APAP, a clinically relevant drug is associated with DILI due to

https://doi.org/10.1021/cbmi.4c00056
Chem. Biomed. Imaging 2025, 3, 77−84

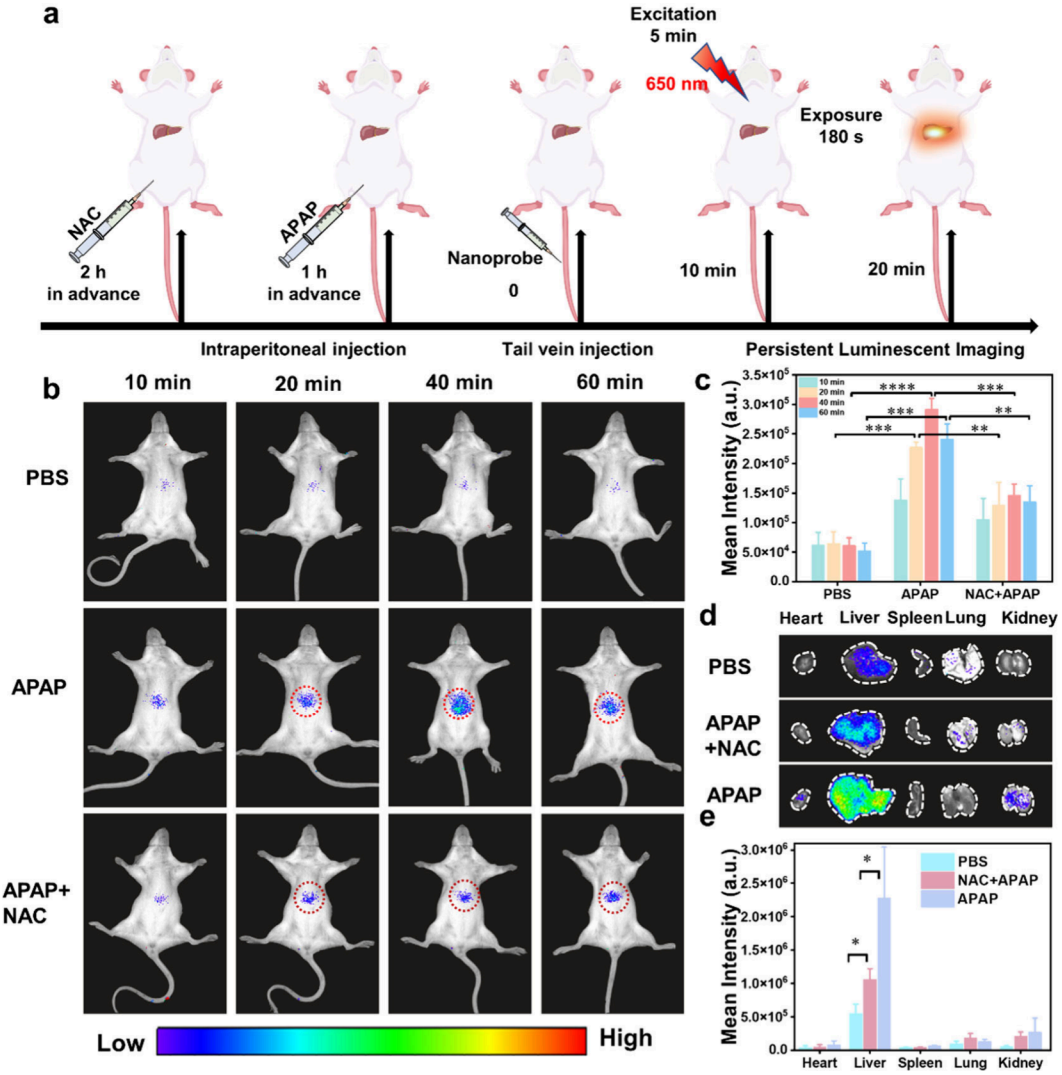

Figure 3. (a) Construction of the DILI mouse model. (b) Time-dependent changes in fluorescence imaging in mice from the PBS group, APAP group, and various APAP+NAC groups (excitation with a 659 nm LED for 5 min prior to each imaging, imaging for 300 s). (c) Time-dependent changes in liver fluorescence intensity in mice from different groups (n = 3). ****p < 0.0001, ***p < 0.001, **p < 0.01, n = 3. (d) Fluorescence intensity in the heart, liver, spleen, lung, and kidney in different groups. (e) Average fluorescence intensity after removal of major organs (n = 3), *p < 0.05, n = 3.

its capacity to drive the occurrence of cellular mitochondrial oxidative stress, during which a large number of ROS are produced.[24,25] Consequently, APAP-induced liver injury serves as an ideal model for investigating cellular oxidative stress potential.[25,26] And NAC is a choice drug for the treatment of drug-induced liver injury.[27−29] Thus, the imaging capability of the ZGGO:Cr-Fc nanoprobe was evaluated in an APAP-induced liver injury cell model (Figure 2a). As shown in Figure 2b, fluorescence imaging revealed enhanced fluorescence intensity in HepG2 cells after APAP treatment compared to the control group. Pretreating the cells with NAC decreased the fluorescence intensity compare to APAP group. Meanwhile, statistical analysis was conducted on the fluorescence intensity of cells in different groups, providing support for the imaging results. These results demonstrated that the ZGGO:Cr-Fc nanoprobe exhibited the ability to detect endogenous H_2O_2 in the APAP-induced liver injury cell model. (Figure 2c).

In order to further investigate the in vivo imaging potential, it is imperative to verify the biological safety of the ZGGO:Cr-Fc nanoprobe. First, a CCK-8 assay was performed to evaluate the cytotoxicity of ZGGO:Cr-Fc on MCF-10A, AML12 and HepG2 cells. Our findings reveal no significant toxicity following 24 h of incubation with varying concentrations of ZGGO:Cr-Fc (Figure 2d,e and Figure S11).Then, hemolysis assays revealed that even at a high concentration of 200 μg/mL, the nanoprobe exhibited a hemolysis rate below 1%, indicating minimal hemotoxicity of ZGGO:Cr-Fc (Figure S12). Additionally, the biodistribution of the ZGGO:Cr-Fc nanoprobe was assessed by employing inductively coupled plasma mass spectrometry (ICP-MS). The results revealed that the nanoprobe primarily accumulated in the liver and lungs, with peak concentration observed at 3 h postinjection, gradually diminishing over time (Figure S13). Then, histological analysis of major organs in healthy mice injected with the ZGGO:Cr-Fc nanoprobe, as compared to a control group receiving saline injections, revealed no significant pathological abnormalities (Figure S14). These findings substantiate the excellent biocompatibility of the ZGGO:Cr-Fc nanoprobe.

https://doi.org/10.1021/cbmi.4c00056
Chem. Biomed. Imaging 2025, 3, 77−84

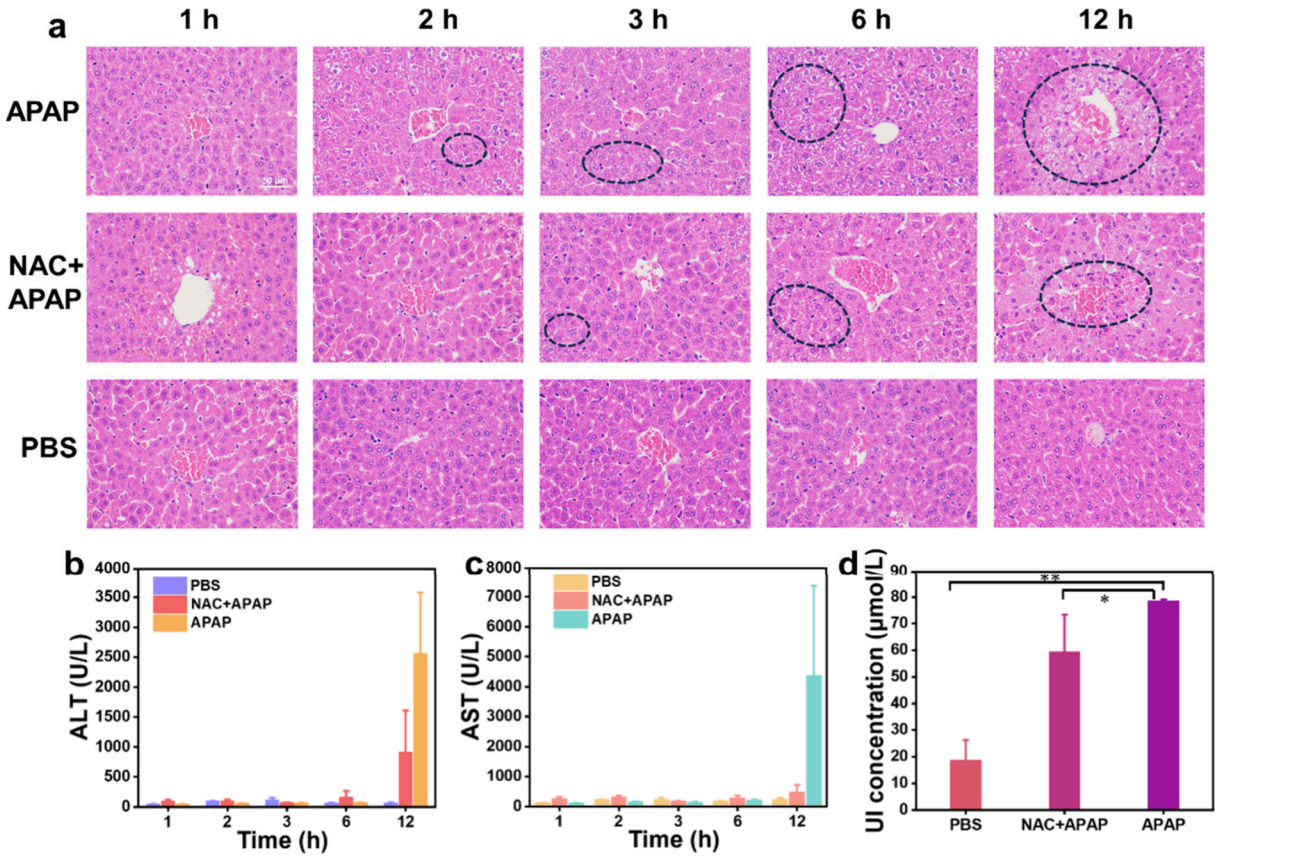

Figure 4. (a) Histological liver sections stained with HE staining from mice in different groups (n = 3), scale bar = 50 μm. (b, c) Time-dependent changes in serum ALT and AST levels in different groups of mice. (d) Urinary iron ion concentrations in different groups (n = 3), $^{**}p < 0.01$.

In Vivo DILI Mouse Imaging

The capability of ZGGO:Cr-Fc nanoprobe to detect endogenous H_2O_2 in living cells has been experimentally validated. Then we investigated the imaging diagnostic capabilities of ZGGO:Cr-Fc nanoprobes in a DILI mouse. APAP is known to induce DILI more effectively in mice than other drugs, making it a suitable model for studying liver injury and recovery that closely resembles human pathological physiology.[25,30,31] Thus, in this study, DILI was induced in mice by intraperitoneal administration of APAP (300 mg/kg) in the DILI group, while the control group received an equivalent dose of PBS. In the treatment group, NAC was administered to one treatment group 1 h prior to APAP injection (150 mg/kg). Subsequently, we employed the ZGGO:Cr-Fc nanoprobes for liver injury imaging (Figure 3a). As shown in Figure 3b, the imaging results of the control, APAP-treated and NAC-treated groups were recorded at 10, 20, 40, and 60 min after intravenous injection. The fluorescence intensity in the liver region of the control group remained consistently weak and unaltered throughout the duration of the experiment. In contrast, APAP-treated mice exhibited a significant increase in liver fluorescence intensity starting at 20 min postinjection, reaching its peak at 40 min, with an impressive signal-to-noise ratio of 20.9. NAC-treated mice also showed a slight enhancement in liver fluorescence intensity from 20 min onward, significantly lower than that observed in APAP-treated group (Figure 3b,c). Furthermore, at 60 min after injection of ZGGO:Cr-Fc nanoprobes, different groups of mice organs (heart, liver, spleen, lungs, and kidneys) were removed, and the fluorescence intensity was measured. As shown in Figure 3d and e, the fluorescence intensity in the liver was significantly higher than in other organs. Notably, the APAP group exhibited a more pronounced fluorescence signal compared to both the NAC-treated and healthy groups, which is consistent with the findings from our in vivo imaging analysis. These results demonstrated that the persistent luminescence nanoprobe enables highly sensitive detection of liver injury and evaluation of therapeutic efficacy.

Serum Enzyme Assay and Histological Analysis of Mice

We further conducted histological analysis on liver tissues from mice treated with APAP and NAC at different time points (Figure 4a). The liver tissue sections from the control group remained histologically normal throughout the experiment, without any vacuolation or other abnormalities. In contrast, the APAP group exhibited progressive liver damage over time, characterized by nuclear cytoplasmic separation and extensive vacuolation. Similarly, the NAC-treated group showed a similar trend but with significantly milder damage, indicating consistent results between tissue staining and imaging findings. Additionally, we performed serum liver function tests on different groups of mice and observed that ALT and AST levels in all mice remained within the normal range for the first 6 h after drug administration (Figure 4b,c and Figure S15). At 12 h post-treatment, there was a significant increase in ALT and AST levels in APAP-treated group, indicative of liver injury. Compared to ALT/AST levels, ZGGO:Cr-Fc nanoprobes enabled early detection of changes in fluorescence signals almost 10 h earlier, demonstrating their high sensitivity imaging capabilities for early detecting liver injury.

https://doi.org/10.1021/cbmi.4c00056
Chem. Biomed. Imaging 2025, 3, 77−84

On the other hand, when H_2O_2 is present, the Fenton reaction occurs in the body, leading to the production of hydroxyl radicals that cleave DNA chains and release iron ions. We tested the concentration of urinary iron ions and found that the levels in the urine of mice in APAP-treated and NAC-treated groups were higher than normal mice (Figure 4d). And the APAP-treated group had higher urinary iron ion concentrations than the NAC-treated group, indicating a correlation between urinary iron ion concentration and the severity of liver injury. The results confirmed that the analysis of urinary iron ions in this study can provide additional insights into the extent of liver injury.

CONCLUSION

In summary, we have successfully developed a novel approach for early diagnosis of DILI using ZGGO:Cr-Fc persistent luminescence nanoprobes that exhibit specific responsiveness to H_2O_2. This approach exhibits exceptional optical stability and biosecurity, yielding a signal-to-noise ratio of up to 20.9 during liver injury imaging in mice. Importantly, in a murine model of hepatic injury, the utilization of persistence luminescence imaging for liver damage diagnosis enables the detection of injury approximately 10 h earlier than the standard clinical serum testing methods. Additionally, the DNA strand on the ZGGO:Cr-Fc nanoprobe caused by liver injury is broken, resulting in the separation of ferrocene loaded on the nanoprobe and its metabolism into the urine through the kidney, which increases the content of iron ions in urine, and can indicate the occurrence of liver injury. These results suggest that the smart persistent luminescence-based approach holds promising potential as a valuable tool for early diagnosis of DILI.

ASSOCIATED CONTENT

Supporting Information

The Supporting Information is available free of charge at https://pubs.acs.org/doi/10.1021/cbmi.4c00056.

Additional experiments, synthesis and characterization, experimental procedures, and original spectra of synthesized compounds (PDF)

AUTHOR INFORMATION

Corresponding Authors

Yun Zhang − *State Key Laboratory of Structural Chemistry, Fujian Institute of Research on the Structure of Matter, Chinese Academy of Sciences, Fuzhou, Fujian 350002, P. R. China; Xiamen Key Laboratory of Rare Earth Photoelectric Functional Materials, Xiamen Institute of Rare Earth Materials, Haixi Institute, Chinese Academy of Sciences, Xiamen, Fujian 361021, P. R. China; Fujian Science and Technology Innovation Laboratory for Optoelectronic Information of China, Fuzhou 350108, P. R. China; University of Chinese Academy of Sciences, Beijing 100049, P. R. China;* orcid.org/0000-0001-6288-4671; Email: zhangy@fjirsm.ac.cn

Quan Yuan − *College of Chemistry and Molecular Sciences, Key Laboratory of Biomedical Polymers of Ministry of Education, Institute of Molecular Medicine, Renmin Hospital of Wuhan University, School of Microelectronics, Wuhan University, Wuhan 430072, P. R. China; Molecular Science and Biomedicine Laboratory (MBL), State Key Laboratory of Chemo/Biosensing and Chemometrics, College of Chemistry and Chemical Engineering, Hunan University, Changsha 410082, P. R. China;* orcid.org/0000-0002-3085-431X; Email: yuanquan@whu.edu.cn

Liang Song − *State Key Laboratory of Structural Chemistry, Fujian Institute of Research on the Structure of Matter, Chinese Academy of Sciences, Fuzhou, Fujian 350002, P. R. China; Xiamen Key Laboratory of Rare Earth Photoelectric Functional Materials, Xiamen Institute of Rare Earth Materials, Haixi Institute, Chinese Academy of Sciences, Xiamen, Fujian 361021, P. R. China; Fujian Science and Technology Innovation Laboratory for Optoelectronic Information of China, Fuzhou 350108, P. R. China; University of Chinese Academy of Sciences, Beijing 100049, P. R. China;* orcid.org/0009-0001-9751-6649; Email: songliang@fjirsm.ac.cn

Authors

Feng Zhang − *State Key Laboratory of Structural Chemistry, Fujian Institute of Research on the Structure of Matter, Chinese Academy of Sciences, Fuzhou, Fujian 350002, P. R. China; Xiamen Key Laboratory of Rare Earth Photoelectric Functional Materials, Xiamen Institute of Rare Earth Materials, Haixi Institute, Chinese Academy of Sciences, Xiamen, Fujian 361021, P. R. China; University of Chinese Academy of Sciences, Beijing 100049, P. R. China*

Ye Lin − *State Key Laboratory of Structural Chemistry, Fujian Institute of Research on the Structure of Matter, Chinese Academy of Sciences, Fuzhou, Fujian 350002, P. R. China; Xiamen Key Laboratory of Rare Earth Photoelectric Functional Materials, Xiamen Institute of Rare Earth Materials, Haixi Institute, Chinese Academy of Sciences, Xiamen, Fujian 361021, P. R. China; University of Chinese Academy of Sciences, Beijing 100049, P. R. China*

Zhengxia Yang − *State Key Laboratory of Structural Chemistry, Fujian Institute of Research on the Structure of Matter, Chinese Academy of Sciences, Fuzhou, Fujian 350002, P. R. China; Xiamen Key Laboratory of Rare Earth Photoelectric Functional Materials, Xiamen Institute of Rare Earth Materials, Haixi Institute, Chinese Academy of Sciences, Xiamen, Fujian 361021, P. R. China; University of Chinese Academy of Sciences, Beijing 100049, P. R. China*

Junpeng Shi − *State Key Laboratory of Structural Chemistry, Fujian Institute of Research on the Structure of Matter, Chinese Academy of Sciences, Fuzhou, Fujian 350002, P. R. China; Xiamen Key Laboratory of Rare Earth Photoelectric Functional Materials, Xiamen Institute of Rare Earth Materials, Haixi Institute, Chinese Academy of Sciences, Xiamen, Fujian 361021, P. R. China; University of Chinese Academy of Sciences, Beijing 100049, P. R. China;* orcid.org/0000-0001-9258-2412

Complete contact information is available at: https://pubs.acs.org/10.1021/cbmi.4c00056

Notes

The authors declare no competing financial interest.

ACKNOWLEDGMENTS

This work was supported by the National Natural Science Foundation of China (62105333), the Young Elite Scientist Sponsorship Program by CAST (YESS20210116), the Fujian Science & Technology Innovation Laboratory for Optoelec-

tronic Information of China (2020ZZ114), and the major science and technology project of Xiamen (3502Z20231014).

REFERENCES

(1) Andrade, R. J.; Chalasani, N.; Björnsson, E. S.; Suzuki, A.; Kullak-Ublick, G. A.; Watkins, P. B.; Devarbhavi, H.; Merz, M.; Lucena, M. I.; Kaplowitz, N.; Aithal, G. P. Drug-induced liver injury. *Nat. Rev. Dis. Primers.* **2019**, *5* (1), 58.

(2) Devarbhavi, H.; Aithal, G.; Treeprasertsuk, S.; Takikawa, H.; Mao, Y.; Shasthry, S. M.; Hamid, S.; Tan, S. S.; Philips, C. A.; George, J.; Jafri, W.; Sarin, S. K. Drug-induced liver injury: Asia Pacific Association of Study of Liver consensus guidelines. *Hepatol. Int.* **2021**, *15* (2), 258−282.

(3) Russmann, S.; Kullak-Ublick, G. A.; Grattagliano, I. Current Concepts of Mechanisms in Drug-Induced Hepatotoxicity. *Curr. Med. Chem.* **2009**, *16* (23), 3041−3053.

(4) Brinker, A. D.; Lyndly, J.; Tonning, J.; Moeny, D.; Levine, J. G.; Avigan, M. I. Profiling Cumulative Proportional Reporting Ratios of Drug-Induced Liver Injury in the FDA Adverse Event Reporting System (FAERS) Database. *Drug Safety.* **2013**, *36* (12), 1169−1178.

(5) Van Swelm, R. P.; Kramers, C.; Masereeuw, R.; Russel, F. G. Application of urine proteomics for biomarker discovery in drug-induced liver injury. *Crit Rev. Toxicol* **2014**, *44* (10), 823−41.

(6) Liu, X.; He, L.; Gong, X.; Yang, Y.; Cheng, D.; Peng, J.; Wang, L.; Zhang, X.-B.; Yuan, L. Engineering of Reversible Luminescent Probes for Real-Time Intravital Imaging of Liver Injury and Repair. *CCS Chemistry* **2022**, *4* (1), 356−368.

(7) Tamber, S. S.; Bansal, P.; Sharma, S.; Singh, R. B.; Sharma, R. Biomarkers of liver diseases. *Mol. Biol. Rep.* **2023**, *50* (9), 7815−7823.

(8) Peng, J.; Samanta, A.; Zeng, X.; Han, S.; Wang, L.; Su, D.; Loong, D. T. B.; Kang, N.-Y.; Park, S.-J.; All, A. H.; Jiang, W.; Yuan, L.; Liu, X.; Chang, Y.-T. Real-Time In vivo Hepatotoxicity Monitoring through Chromophore-Conjugated Photon-Upconverting Nanoprobes. *Angew. Chem., Int. Ed.* **2017**, *56* (15), 4165−4169.

(9) Chen, S.; Pan, H.; Chen, Y.; Lu, L.; He, X.; Chen, H.; Chen, R.; Zhan, S.; Tang, S. Association between genetic polymorphisms of NRF2, KEAP1, MAFF, MAFK and anti-tuberculosis drug-induced liver injury: a nested case-control study. *Sci. Rep.* **2019**, *9* (1), 14311.

(10) Cheng, D.; Xu, W.; Gong, X.; Yuan, L.; Zhang, X.-B. Design Strategy of Fluorescent Probes for Live Drug-Induced Acute Liver Injury Imaging. *Acc. Chem. Res.* **2021**, *54* (2), 403−415.

(11) Villanueva-Paz, M.; Morán, L.; López-Alcántara, N.; Freixo, C.; Andrade, R. J.; Lucena, M. I.; Cubero, F. J. Oxidative Stress in Drug-Induced Liver Injury (DILI): From Mechanisms to Biomarkers for Use in Clinical Practice. *Antioxidants.* **2021**, *10*, 390.

(12) Sun, D.; Chen, Z.; Hu, J.; Zeng, H.; Qu, L.; Yang, R. Recent advance of fluorescent probes for detection of drug-induced liver injury markers. *Chin. Chem. Lett.* **2022**, *33* (10), 4478−4494.

(13) Shuhendler, A. J.; Pu, K.; Cui, L.; Uetrecht, J. P.; Rao, J. Real-time imaging of oxidative and nitrosative stress in the liver of live animals for drug-toxicity testing. *Nat. Biotechnol.* **2014**, *32* (4), 373−380.

(14) Chen, J.; Chen, L.; Wu, Y.; Fang, Y.; Zeng, F.; Wu, S.; Zhao, Y. A H_2O_2-activatable nanoprobe for diagnosing interstitial cystitis and liver ischemia-reperfusion injury via multispectral optoacoustic tomography and NIR-II fluorescent imaging. *Nat. Commun.* **2021**, *12* (1), 6870.

(15) Zuo, Q.; Wu, Q.; Lv, Y.; Gong, X.; Cheng, D. Imaging of endoplasmic reticulum superoxide anion fluctuation in a liver injury model by a selective two-photon fluorescent probe. *New J. Chem.* **2020**, *44* (14), 5457−5462.

(16) Tian, Y.; Liu, S.; Cao, W.; Wu, P.; Chen, Z.; Xiong, H. H_2O_2-Activated NIR-II Fluorescent Probe with a Large Stokes Shift for High-Contrast Imaging in Drug-Induced Liver Injury Mice. *Anal. Chem.* **2022**, *94* (32), 11321−11328.

(17) Wang, N.; Yang, Y.; Zhang, M.; Zhu, Q.; Li, Z. *Anal.* Lysosomal Adenosine Triphosphate-Activated Upconversion Nanoparticle/Carbon Dot Composite for Ratiometric Imaging of Hepatotoxicity. *Chem.* **2022**, *94* (45), 15738−15745.

(18) Mi, C.; Guan, M.; Zhang, X.; Yang, L.; Wu, S.; Yang, Z.; Guo, Z.; Liao, J.; Zhou, J.; Lin, F.; et al. High spatial and temporal resolution NIR-IIb gastrointestinal imaging in mice. *Nano Lett.* **2022**, *22* (7), 2793−2800.

(19) Huang, K.; Le, N.; Wang, J. S.; Huang, L.; Zeng, L.; Xu, W.-C.; Li, Z.; Li, Y.; Han, G. Designing Next Generation of Persistent Luminescence: Recent Advances in Uniform Persistent Luminescence Nanoparticles. *Adv. Mater.* **2022**, *34* (14), 2107962.

(20) Chen, Z.-Z.; Wang, L.-C.; Manoharan, D.; Lee, C.-L.; Wu, L.-C.; Huang, W.-T.; Huang, E.-Y.; Su, C.-H.; Sheu, H.-S.; Yeh, C.-S. Low Dose of X-Ray-Excited Long-Lasting Luminescent Concave Nanocubes in Highly Passive Targeting Deep-Seated Hepatic Tumors. *Adv. Mater.* **2019**, *31* (49), 1905087.

(21) Zhao, H.; Liu, C.; Gu, Z.; Dong, L.; Li, F.; Yao, C.; Yang, D. Persistent Luminescent Nanoparticles Containing Hydrogels for Targeted, Sustained, and Autofluorescence-Free Tumor Metastasis Imaging. *Nano Lett.* **2020**, *20* (1), 252−260.

(22) Abdukayum, A.; Chen, J.-T.; Zhao, Q.; Yan, X.-P. Functional Near Infrared-Emitting Cr^{3+}/Pr^{3+} Co-Doped Zinc Gallogermanate Persistent Luminescent Nanoparticles with Superlong Afterglow for in Vivo Targeted Bioimaging. *J. Am. Chem. Soc.* **2013**, *135* (38), 14125−14133.

(23) Yu, M.; Ye, Z.; Liu, S.; Zhu, Y.; Niu, X.; Wang, J.; Ao, R.; Huang, H.; Cai, H.; Liu, Y.; Chen, X.; Lin, L. Redox-Active Ferrocene Quencher-Based Supramolecular Nanomedicine for NIR-II Fluorescence-Monitored Chemodynamic Therapy. *Angew. Chem., Int. Ed.* **2024**, *63* (10), e202318155.

(24) Budnitz, D. S.; Lovegrove, M. C.; Crosby, A. E. Emergency Department Visits for Overdoses of Acetaminophen-Containing Products. *Am. J. Prev. Med.* **2011**, *40* (6), 585−592.

(25) Jaeschke, H.; Xie, Y.; McGill, M. R. Acetaminophen-induced Liver Injury: from Animal Models to Humans. *J. Clin Transl Hepatol* **2014**, *2* (3), 153−161.

(26) Wang, H.; Zhang, R.; Bridle, K. R.; Jayachandran, A.; Thomas, J. A.; Zhang, W.; Yuan, J.; Xu, Z. P.; Crawford, D. H. G.; Liang, X.; Liu, X.; Roberts, M. S. Two-photon dual imaging platform for in vivo monitoring cellular oxidative stress in liver injury. *Sci. Rep.* **2017**, *7* (1), 45374.

(27) Downs, J. W.; Cumpston, K. L.; Kershner, E. K.; Troendle, M. M.; Rose, S. R.; Wills, B. K. Clinical outcome of massive acetaminophen overdose treated with standard-dose N-acetylcysteine. *Clin. Toxicol.* **2021**, *59* (10), 932−936.

(28) Saito, C.; Zwingmann, C.; Jaeschke, H. Novel mechanisms of protection against acetaminophen hepatotoxicity in mice by glutathione and N-acetylcysteine. *Hepatology* **2010**, *51* (1), 246−254.

(29) Zhou, C.; Zhang, L.; Xu, Z.; Sun, T.; Gong, M.; Liu, Y.; Zhang, D. Self-Propelled Ultrasmall AuNPs-Tannic Acid Hybrid Nanozyme with ROS-Scavenging and Anti-Inflammatory Activity for Drug-Induced Liver Injury Alleviation. *Small* **2023**, *19* (19), 2206408.

(30) Lee, K. C. L.; Palacios Jimenez, C.; Alibhai, H.; Chang, Y.-M.; Leckie, P. J.; Baker, L. A.; Stanzani, G. L.; Priestnall, S.; Mookerjee, R. P.; Jalan, R.; Davies, N. A. A reproducible, clinically relevant, intensively managed, pig model of acute liver failure for testing of therapies aimed to prolong survival. *Liver Int.* **2013**, *33* (4), 544−551.

(31) Cheng, D.; Peng, J.; Lv, Y.; Su, D.; Liu, D.; Chen, M.; Yuan, L.; Zhang, X. Design of Chemical Stability Near-Infrared Molecular Probes for High-Fidelity Hepatotoxicity Evaluation In Vivo. *J. Am. Chem. Soc.* **2019**, *141* (15), 6352−6361.

https://doi.org/10.1021/cbmi.4c00056
Chem. Biomed. Imaging 2025, 3, 77−84